Device operation of P-ion-implanted n-$BaSi_2$/p-Si heterojunction solar cells

Aonuki, Sho; Yamashita, Yudai; Limodio, Gianluca; Narita, Shunsuke; Takayanagi, Kaori; Iwai, Ai; Toko, Kaoru; Zeman, Miro; Isabella, Olindo; Suemasu, Takashi

DOI
10.1002/pip.3658

Publication date
2022

Document Version
Final published version

Published in
Progress in Photovoltaics: research and applications

Received: 30 June 2022 | Revised: 20 November 2022 | Accepted: 1 December 2022

DOI: 10.1002/pip.3658

APPLICATIONS

PROGRESS IN PHOTOVOLTAICS WILEY

Device operation of P-ion-implanted n-$BaSi_2$/p-Si heterojunction solar cells

Sho Aonuki[1] | Yudai Yamashita[1] | Gianluca Limodio[2] | Shunsuke Narita[1] | Kaori Takayanagi[1] | Ai Iwai[1] | Kaoru Toko[3] | Miro Zeman[2] | Olindo Isabella[2] | Takashi Suemasu[3]

[1]Graduate School of Science and Technology, University of Tsukuba, Tsukuba, Japan

[2]Photovoltaic Materials and Device Group, Delft University of Technology, Delft, The Netherlands

[3]Department of Applied Physics, Faculty of Pure and Applied Sciences, University of Tsukuba, Tsukuba, Japan

Correspondence
Takashi Suemasu, Department of Applied Physics, Faculty of Pure and Applied Sciences, University of Tsukuba, Tsukuba 305-8573, Japan.
Email: suemasu.takashi.gu@u.tsukuba.ac.jp

Funding information
JSPS KAKENHI (Grants 19KK0104 and JP21H04548). Grant-in-Aids for JSPS Research Fellowships for Young Scientists (Grant 21J20404 and 19J21372). Science Grant Agency of the Ministry of Education, Science, Research and Sport of the Slovak Republic for financial support of projects VEGA 1/0532/19 and VEGA 1/0529/20.

Abstract

We formed phosphorous(P)-ion-implanted n-$BaSi_2$ films on p-Si(111) substrates and demonstrated solar-cell functionality of the n-$BaSi_2$/p-Si heterojunction under AM1.5 illumination. The $BaSi_2$ films were grown by molecular beam epitaxy, followed by implantation of P ions to the $BaSi_2$ films using PF_3 gas at an energy of 10 keV and a dose of 1×10^{14} cm^{-2}. Subsequent postannealing was conducted at 500°C in Ar for different durations (t = 30–480 s) to activate the P atoms. The diffusion coefficient for P atoms in $BaSi_2$ was evaluated from the depth profiles of P atoms by secondary-ion mass spectrometry. The activation energies of lattice and grain boundary diffusion were found to be 1.1 ± 0.6 and 2.5 ± 0.6 eV, respectively. From the analysis of Raman and photoluminescence spectra, the ion implantation damage was recovered by the postannealing. For one treated sample with t = 120 s, the internal quantum efficiency reached 67% at a wavelength of 870 nm. This is the highest ever achieved for n-$BaSi_2$/p-Si heterojunction solar cells. Ion implantation is thus applicable to $BaSi_2$ films grown by any other method. This achievement thereby opens a new route for the formation of $BaSi_2$ solar cells.

KEYWORDS
$BaSi_2$, ion implantation, solar cell

1 | INTRODUCTION

Photovoltaic systems consisting of safe, stable, and earth-abundant materials play an important role in realizing a decarbonized society. Crystalline Si (c-Si) solar cells currently account for approximately 95% of the solar cell market[1]; their conversion efficiency (η) exceeds 26% at laboratory levels.[2–5] However, the installation of c-Si solar panels is limited to mostly flat and stable places due to their weight and nonflexibility. For further deployment of solar cells, thin-film and flexible solar-cell materials such as Cu(In,Ga)$(Se,S)_2$, CdTe, and perovskite have attracted a growing interest through low-cost growth processes and high η of over 22%.[6–12] Under these circumstances, we have paid special attention to $BaSi_2$, which is a semiconducting silicide composed of only earth-abundant elements.[13,14]

$BaSi_2$ is an indirect band-gap semiconductor with a band gap of 1.3 eV, which is suitable for solar-cell applications. Because $BaSi_2$ has a direct transition edge only 0.1 eV above the band gap,[15] both a large absorption coefficient (3×10^4 cm^{-1} at 1.5 eV) and an excellent minority carrier diffusion length (10 μm) are achievable.[16–18] Solar-cell materials possessing such features are quite limited. These properties meet the requirement for high-efficiency thin-film solar cells. To date, solar-cell functionality of p-$BaSi_2$/n-Si heterojunctions,[19–21] $BaSi_2$ homojunction,[22] and n^+-AZO/p-$BaSi_2$ heterojunction[23] has been demonstrated on Si substrates. Among them, p-$BaSi_2$/n-Si solar cells formed by molecular beam epitaxy (MBE) and by vacuum evaporation exhibited η = 9.9%[19] and 10.62%,[24] respectively. In regard to $BaSi_2$ homojunction solar cells, however, the highest η ever achieved is as small as 0.28%[25] although simulations expected η > 25%.[26] Since

polycrystalline $BaSi_2$ films with high-photoresponsivity can now be formed on glass substrate by sputtering,[27] $BaSi_2$ thin-film solar cells can be targeted. The problem with $BaSi_2$ homojunction solar cells is the difficulty in forming an abrupt pn-junction because of their large diffusion coefficient and the high vapor pressure of Sb adopted as an n-type impurity for $BaSi_2$.[28] Therefore, the low-temperature MBE growth of Sb-doped n-$BaSi_2$ at ~500°C, ~150°C lower than that for $BaSi_2$ light-absorber layers, is indispensable to ensure an electron concentration of over 10^{18} cm^{-3}.[29] These factors degrade the crystalline quality of layered structure, resulting in low η. Therefore, it is necessary to explore other n-type dopants instead of Sb and doping method.

The valence band maximum of $BaSi_2$ primarily consists of Si 3s and 3p orbitals[30–33]; therefore, replacement of some of the Si atoms in $BaSi_2$ with group 15 elements such as P, As, and Sb increases the electron concentration of $BaSi_2$. We have also succeeded in controlling electron concentrations through MBE using As in the role of n-type impurity[34,35] and achieved high photoresponsivity of As-doped n-$BaSi_2$ films by atomic H treatment.[36,37] However, the conductivity type of As-doped $BaSi_2$ films sometimes switches from n-type to p-type.[37] Among P, As, and Sb, P is not easy to handle by sputtering or MBE methods because of its high vapor pressure and reactivity. This has led to very limited research on P-doped $BaSi_2$ films. For this reason, we chose the ion implantation method and P as an n-type dopant for $BaSi_2$ in this work. Implantation of P ions is also useful to control electron concentrations in $BaSi_2$,[38,39] yielding concentrations up to 10^{18} cm^{-3}.[38,40] However, the solar-cell application of P-ion-implanted n-$BaSi_2$ has not been reported. We also chose a simple $BaSi_2$/Si heterojunction structure so that we could focus our discussion only on the implanted $BaSi_2$ layers. For these reasons, we fabricated P-ion-implanted n-$BaSi_2$/p-Si heterojunction solar cells as the first application of P-ion-implanted n-$BaSi_2$ to an electron transport layer in this work. It is noted that the η of n-$BaSi_2$/p-Si is intrinsically quite limited. Figure 1A shows the band alignment of $BaSi_2$ and Si with respect to the vacuum level, and Figure 1B shows the band alignment of an n-$BaSi_2$ (60 nm, $n = 1.5 \times 10^{18}$ cm^{-3})/p-Si ($p = 1.0 \times 10^{16}$ cm^{-3}) diode calculated using AFORS-HET.[41] For the calculations, parameters such as the effective density of states of the conduction band for $BaSi_2$ ($N_C = 2.0 \times 10^{19}$ cm^{-3})[30] were used. The electron concentration (n) and hole concentration (p) are tailored to the experiment described later. At the $BaSi_2$/Si heterointerface, there is a large conduction band offset for photogenerated electrons in the p-Si substrate to travel to the n-$BaSi_2$ layer due to a small electron affinity of $BaSi_2$ (~3.2 eV)[42] and a large valence band offset for photogenerated holes in the n-$BaSi_2$ layer to be transferred into the p-Si substrate. Such large band offsets hinder the transport of photogenerated carriers across the hetero-interface.[22] The goal of this study is therefore not to achieve high η but to form the n-$BaSi_2$/p-Si diode to assess the feasibility of ion implantation in $BaSi_2$ solar cells.

2 | EXPERIMENTAL METHOD

Prior to the fabrication of P-ion-implanted n-$BaSi_2$/p-Si heterojunction solar cells, we evaluated the diffusion coefficient of P atoms in the lattice and grain boundary (GB) of $BaSi_2$. For this purpose, we fabricated 570-nm-thick undoped $BaSi_2$ films on floating-zone (FZ) n-Si (111) substrates (resistivity ρ > 1000 Ω cm) through MBE (AVC Co., Ltd.) with a Knudsen cell for Ba and an electron-beam gun for Si. Details of the growth procedure have been reported previously.[43–45] After that, a-Si capping layers with a thickness of 3 nm were formed in situ to suppress oxidation of $BaSi_2$.[46] P ions were implanted in the $BaSi_2$ films using PF_3 gas at an ion injection energy of 5 keV and a dose of 10^{15} cm^{-2}. These samples were annealed at 500–600°C for 3–30 min in an Ar atmosphere using a rapid-thermal-annealing system (ULVAC MILA-5000UHV). The depth profile of the P atoms in $BaSi_2$ was investigated in secondary-ion mass spectrometry (SIMS) employing Cs^+ ions.

Next, we formed undoped $BaSi_2$ films on FZ p-Si(111) substrates (ρ > 1000 Ω cm) to characterize the properties of P-ion-implanted $BaSi_2$ films and the Czochralski p-Si(111) substrate (ρ = 1–4 Ω cm) used in fabricating the $BaSi_2$/Si heterojunction solar cells by the procedure described above. The thicknesses of the $BaSi_2$ films were 200 and 60 nm, respectively. P ions were implanted in the $BaSi_2$ films using PF_3 gas at an ion injection energy of 10 keV and a dose of 10^{14} cm^{-2}. Preannealing and sacrificial $BaSi_2$ films on the Si substrates were employed to prevent oxidation of the $BaSi_2$ films using the same procedure reported previously.[47–49] Postannealing was performed at 500°C for 30–480 s in Ar to activate the implanted P atoms and remove the ion implantation damage. For the Hall measurements, 150-nm-thick front Al electrodes with a diameter of 1 mm were

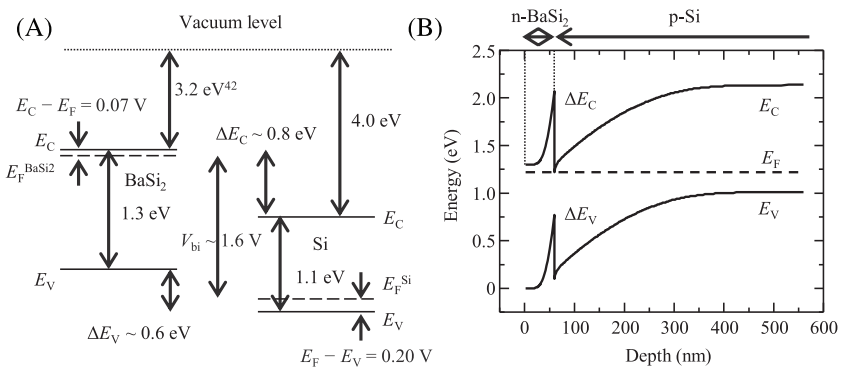

FIGURE 1 (A) Band alignment of $BaSi_2$ and Si with respect to the vacuum level. (B) Calculated band alignment by AFORS-HET for an n-$BaSi_2$(60 nm, $n = 1.5 \times 10^{18}$ cm^{-3})/p-Si ($p = 1.0 \times 10^{16}$ cm^{-3}) diode

formed by sputtering; to investigate solar-cell performance, 80-nm-thick front ITO electrodes with a diameter of 1 mm and a rear Al electrode with a thickness of 150 nm were formed by sputtering. The crystalline quality of the P-ion-implanted $BaSi_2$ films was evaluated using a laser Raman spectrometer (JASCO, NRS-5100) employing a frequency-doubled Nd:YAG laser (532 nm). The Raman shift was calibrated using the transverse optical (TO) phonon line of c-Si (520.2 cm^{-1}).

The optical properties were characterized from photoluminescence (PL) measurements at 8 K. An excitation laser light of 442 nm illuminated the $BaSi_2$ side and the PL spectra was recorded by an InP/InGaAs photomultiplier (Hamamatsu Photonics R5509-72) and amplified using the lock-in-technique. The Van der Pauw method was performed to determine the resistivity and Hall coefficient and thus the conductivity type and carrier concentration.[50] The current density versus voltage (*J*–*V*) curves under AM1.5 illumination were measured to evaluate the P-ion-implanted n-$BaSi_2$/p-Si solar-cell performance. We performed photoresponsivity measurements of the P-ion-implanted n-$BaSi_2$/p-Si solar cells using a Xenon lamp with a 25-cm-focal-length single monochromator (Bunko Keiki SM-1700A and RU-60N) under no bias voltage and reflectance measurements using a reflection measurement system with the xenon lamp and an integrating sphere to obtain the internal quantum efficiency (*IQE*) spectra. The incident light intensity was calibrated using a pyroelectric sensor (Melles Griot 13PEM001/J). The capacitance versus voltage (*C*-*V*) characteristics were measured using a 1-MHz capacitance meter (HP 4280A). All measurements except for the PL spectra were conducted at room temperature.

3 | RESULTS AND DISSCUSSION

3.1 | Diffusion coefficient of P atoms in $BaSi_2$

As for the depth profiles of P atoms in $BaSi_2$ films after postannealing at 500°C for 30 min, 550°C for 15 min, and 600°C for 3 min (Figure 2A), we note that the measured P atoms concentration was not precise. Reference sample of $BaSi_2$ controlled P atoms concentration is necessary to calibrate the matrix effect; however, it has not yet been prepared. We therefore adopted for this study P-doped Si instead of $BaSi_2$ as a reference sample; the following analysis is however not affected. We evaluated the coefficient of diffusion P atoms in the lattice (D_l) and the GB (D_{GB}) of $BaSi_2$ by fitting the depth profiles of the P atoms (Figure 2) using fitting functions:

$$C(x,t) = \frac{S}{\sqrt{\pi D_l t}} \exp\left[-\frac{(x-d)^2}{4D_l t}\right], \quad (1)$$

$$s\delta D_{GB} = 1.322\left(\frac{D_l}{t}\right)^{1/2}\left(-\frac{\partial \ln C(x,\ t)}{\partial x^{6/5}}\right)^{-5/3}, \quad (2)$$

which give the concentration distributions of impurity atoms that arise through lattice and GB diffusion, respectively; here, $x = d$ is the center of the as-implanted distribution, S the total amount of impurities, t the annealing time, C_0 the impurity concentration at the initial point of GB diffusion, s the segregation factor of GB, and δ the width of the GB.[51–55] We used Equation (1) to calculate D_l because the total amount of the implanted P atoms in $BaSi_2$ films does not change after annealing. Equation (2) matches the Harrison Type-B kinetics regime corresponding to a condition that the average lattice diffusion length of the impurity atoms is less than the grain size.[51,53,54] According to previous research, the grain size of $BaSi_2$ is approximately 4 μm,[56] much larger than the lattice diffusion length of P atoms in $BaSi_2$ films (~60 nm) calculated from Equation (1), and thus Equation (2) is valid

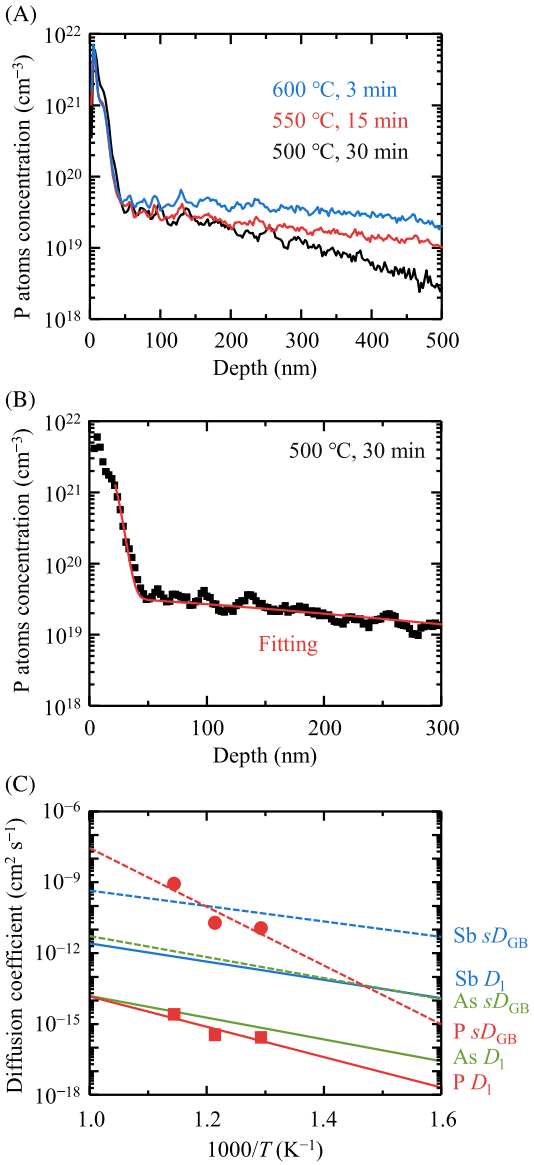

FIGURE 2 (A) SIMS depth profiles of P atoms concentration in $BaSi_2$ films annealed at 500°C for 30 min, 550°C for 15 min, and 600°C for 3 min. (B) Fitting curve by Equations (1) and (2). (C) Lattice and GB diffusion coefficients of P, As, and Sb atoms in $BaSi_2$ [Colour figure can be viewed at wileyonlinelibrary.com]

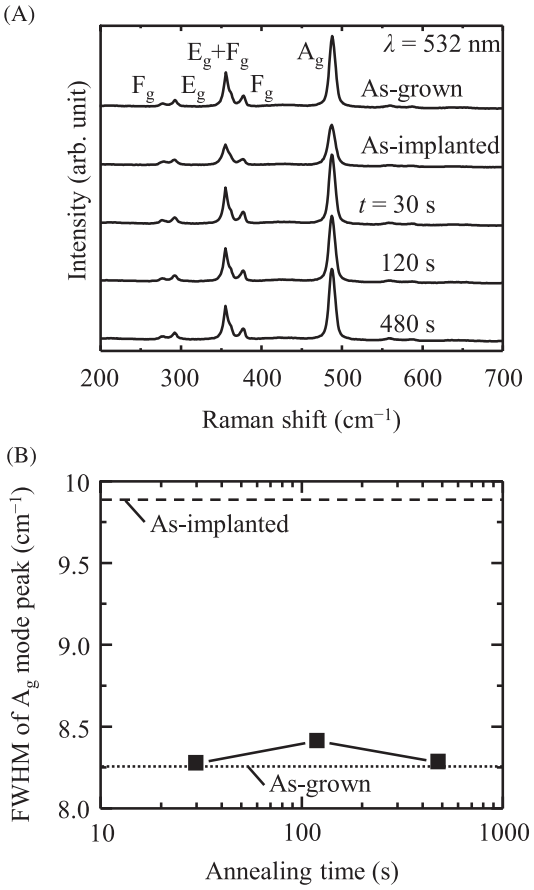

FIGURE 3 (A) Raman spectra of P-ion-implanted and undoped as-grown $BaSi_2$ films annealed for different durations. (B) Full-width at half maximum of A_g mode peak for these samples

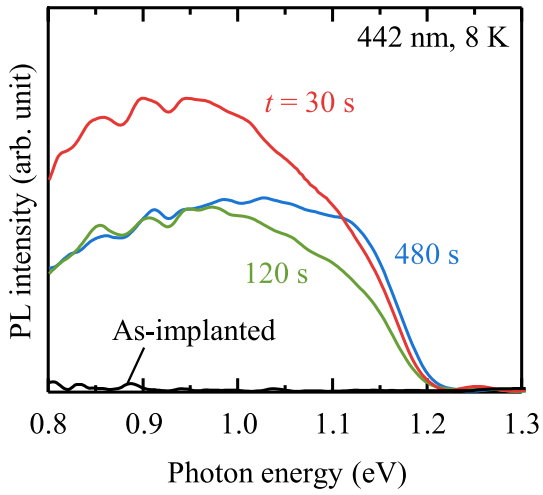

FIGURE 4 PL spectra of P-ion-implanted $BaSi_2$ films with or without postannealing at 500°C for different durations [Colour figure can be viewed at wileyonlinelibrary.com]

in this study. We adopted La Claire's equation[55] to analyze the parallel GB model, which used for the analysis of lattice and GB diffusion coefficient of B, Al, As, and Sb in $BaSi_2$.[28,57–59] We set δ for the $BaSi_2$ films to 0.5 nm because this value is commonly adopted in GB diffusion studies.[60,61] Sharp GBs of the $BaSi_2$ epitaxial films were observed in transmission electron microscopy,[18] indicating that this hypothesis is reasonable.

All the experimental depth profiles of P atoms in $BaSi_2$ films measured by SIMS are well reproduced by Equations (1) and (2), as exemplified in Figure 2B. We performed fittings using Equations (1) and (2) at the same time. Figure 2C shows the Arrhenius plots using the obtained D_I and sD_{GB} of P, As, and Sb atoms in $BaSi_2$.[28,59] The P atoms display the smallest D_I of all studied n-type impurities for $BaSi_2$, whereas the sD_{GB} of P atoms greatly depends on the postannealing temperature, suggesting that the diffusion of P atoms is suppressed by annealing at low temperature compared with As and Sb. Furthermore, we calculated the activation energy E_a of lattice and GB diffusions for P atoms in $BaSi_2$ using

$$D_I = D_I^0 \exp\left(-\frac{E_a}{k_B T}\right), \quad (3)$$

$$sD_{GB} = D_{GB}^0 \exp\left(-\frac{E_a}{k_B T}\right). \quad (4)$$

Here, k_B denotes the Boltzmann constant, and T the absolute temperature. The activation energies for P atoms undergoing lattice and GB diffusion are 1.1 ± 0.6 and 2.5 ± 0.6 eV, respectively. These values are relatively higher than those of As (0.91 and 0.88 eV) and Sb (0.77 and 0.65 eV).[28,59] Generally, activation energies of 0.5–2 eV correspond to interstitial diffusion, whereas those of 3–5 eV relate to vacancy diffusion.[62] This is because the energy of formation for vacancies is also taken into account in determining vacancy diffusion. According to previous research, the energy of formation for Si vacancies is ~1.0 eV[15]; therefore, we speculate that the diffusion of P atoms in $BaSi_2$ corresponds to interstitial diffusion and vacancy diffusion in lattice and GB, respectively. It is noted that the magnitude relationship between the two activation energies for P is different from those for As and Sb. Since it was found that the deposition rate ratio of Ba to Si (R_{Ba}/R_{Si}) during $BaSi_2$ film deposition significantly affects the electrical and photoresponse properties,[63] we have set the value of R_{Ba}/R_{Si} at 2.2, which is different from 3.0 in the previous work.[28,59] This may affect the GB character in $BaSi_2$ films and thereby the magnitude relationship between the two activation energies related to diffusion.

3.2 | Characteristics of P-ion-implanted n-$BaSi_2$ films

From the Raman spectra of P-ion-implanted $BaSi_2$ films (Figure 3A), vibration modes such as A_g, E_g, and F_g stemming from Si tetrahedra in $BaSi_2$ were observed for all samples.[64] After ion implantation, the intensity of these peaks decreased because ion implantation damages

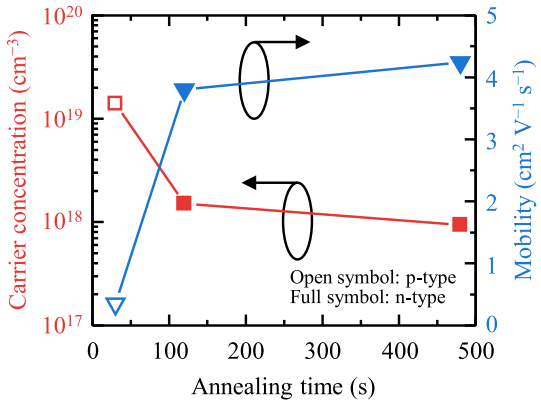

FIGURE 5 Annealing time dependence for carrier concentration and mobility of P-ion-implanted $BaSi_2$ films. Open square and triangle indicate p-type conductivity while full symbols show n-type conductivity. [Colour figure can be viewed at wileyonlinelibrary.com]

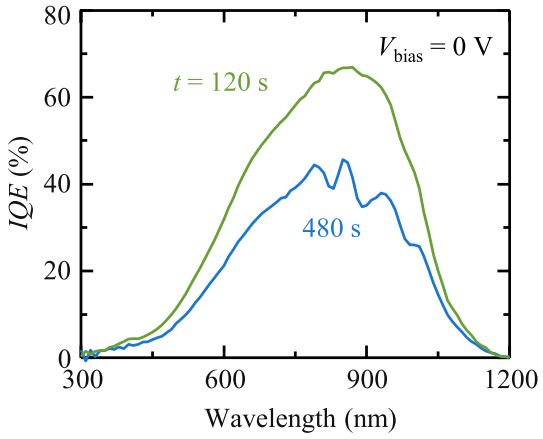

FIGURE 6 *IQE* spectra of P-ion-implanted n-$BaSi_2$/p-Si heterojunction solar cells under no bias voltages [Colour figure can be viewed at wileyonlinelibrary.com]

the crystal structure of $BaSi_2$. Subsequent annealing at 500°C for more than 30 s recovered the intensity of these peaks. The full-width at half-maximum of the A_g mode (Figure 3B) first increases after ion implantation and then decreases after postannealing to almost the same value as that of the as-grown sample. From these results, we infer that the damage from ion implantation is reversible by postannealing at 500°C for at least 30 s.

From the PL spectra of these samples (Figure 4), the PL intensity of the as-implanted sample is almost invisible. From the PL spectra of these samples (Figure 4), the PL intensity of the as-implanted sample is almost invisible. The excitation laser light of 442 nm is mostly absorbed within the 200-nm-thick $BaSi_2$ films due to its high optical absorption coefficient beyond 5×10^5 cm^{-1}. Therefore, the PL spectra in Figure 4 reflect how the photogenerated electrons and holes recombine in $BaSi_2$. Since the $BaSi_2$ films with high photoresponsivity exhibit intense PL originating from electron transitions between localized states within the band gap,[35,65] we can state that the as-implanted sample contained a lot of nonradiative defects. After the postannealing, the PL increased, meaning that such nonradiative defects decreased drastically. Based on these results, postannealing is an effective means to not only improve the crystalline quality of $BaSi_2$ films but also decrease nonradiative defects in the P-ion-implanted $BaSi_2$ films. The broad spectra can be deconvoluted into four peaks, and the PL at around 0.9 eV is associate with Si vacancies.[66] We therefore speculate that the reduction of the 0.9-eV PL is attributable to the occupation of Si vacancies by P atoms.

From the annealing duration dependences of carrier concentration and mobility of P-ion-implanted $BaSi_2$ films (Figure 5), all samples showed n-type conductivity except for the sample annealed for 30 s. We infer that the annealing duration of 30 s was insufficient to activate P atoms. For samples annealed for 30, 120, and 480 s, carrier concentrations were (14.0, 1.5, and 0.93) $\times 10^{18}$ cm^{-3}, respectively. These values are acceptable for electron transport layers of $BaSi_2$ solar cells. The mobility of P-ion-implanted $BaSi_2$ films shows a much lower value than that of MBE-grown Sb- and As-doped $BaSi_2$ films.[29,34]

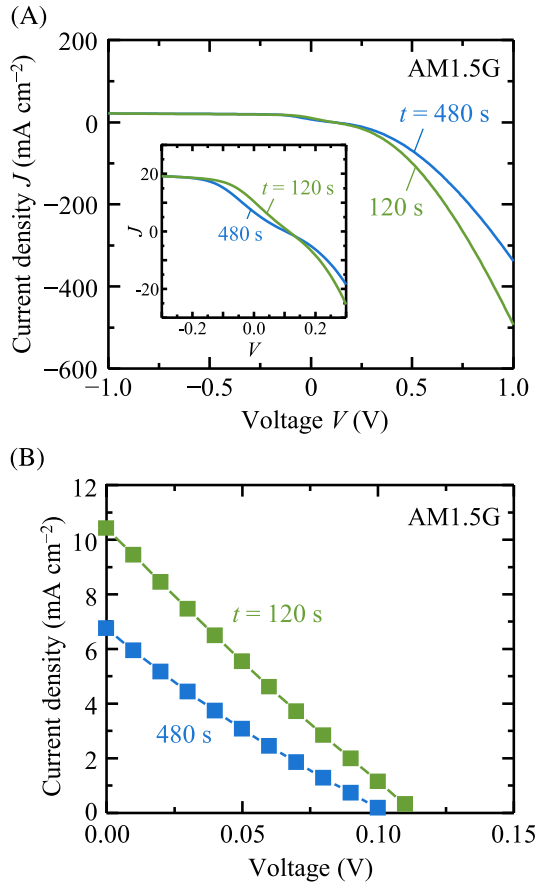

FIGURE 7 (A) *J-V* curves under AM1.5 illumination of P-ion-implanted n-$BaSi_2$/p-Si heterojunction solar cells. The annealing duration is 120 s or 480 s. The inset shows a magnified view at around $V = 0$ V. (B) The first quadrant of the *J-V* curves in (A) [Colour figure can be viewed at wileyonlinelibrary.com]

TABLE 1 Solar-cell parameters and values for the P-ion-implanted n-$BaSi_2$/p-Si heterojunction solar cells annealed for 120 and 480 s. Short-circuit current density J_{SC}, open-circuit voltage V_{OC}, fill factor *FF*, conversion efficiency η, series resistance R_S, shunt resistance R_{SH}, ideal factor γ, and reverse saturation current density J_0 are all tabulated.

t (s)	J_{SC} (mA cm^{-2})	V_{OC} (V)	*FF*	η (%)	R_S (Ω)	R_{SH} (Ω)	γ	J_0 (mA cm^{-2})
120	10	0.11	0.23	0.28	1.1×10^3	4.1×10^4	1.6	6.7×10^{-1}
480	6.7	0.10	0.22	0.15	1.4×10^3	5.7×10^3	2.0	1.1×10^0

3.3 | Solar-cell application of P-ion-implanted n-$BaSi_2$

The *IQE* reached 67% at a wavelength of approximately 900 nm and originated from the Si substrate (see Figure 6). This value is the highest of all the n-$BaSi_2$/p-Si heterojunction solar cells ever reported.[22,67] In addition, the *IQE* in the short wavelength range (< 600 nm) is greater than that for Sb-doped n-$BaSi_2$/p-Si heterojunction solar cells.[22] Because the absorption coefficient of $BaSi_2$ is very high at these wavelengths, most of the short wavelength photons are absorbed in the $BaSi_2$ films. Therefore, this result implies that the photogenerated carriers in the P-ion-implanted n-$BaSi_2$ were extracted in the external circuit.

Figure 7A,B presents the *J*–*V* curves for P-ion-implanted n-$BaSi_2$/p-Si heterojunction solar cells under AM1.5 illumination. Rectification is observed for the ion-implanted n-$BaSi_2$/p-Si diode. To understand what occurs in these devices in more detail, we calculated the solar-cell parameters such as series resistance R_S and the reverse-bias saturation current density J_0 using[68]

$$\frac{dV}{dJ} = SR_S + \frac{\gamma k_B T}{q}\left[\frac{1-(SR_{SH})^{-1}dV/dJ}{J+J_{SC}-(SR_{SH})^{-1}V}\right], \quad (5)$$

where S denotes the device area, γ the diode ideality factor, and R_{SH} the shunt resistance. All the solar-cell parameters and values including fill factor *FF* are listed in Table 1. The samples annealed for 120 and 480 s exhibited η values of 0.28 and 0.15%, respectively. These values are much smaller than that for MBE-grown Sb-doped n-$BaSi_2$/p-Si heterojunction solar cells (1.5%).[22] The main reasons for such small η are defects at the n-$BaSi_2$/p-Si interface, large R_S, and small R_{SH}. As shown in the inset of Figure 7A, the S-shaped *J*-*V* characteristics became noticeable. Such behavior could be due to interface defects and/or band alignment mismatch, preventing the carrier transport across the interface and thus restricting the V_{OC} and the J_{SC}.[69–71] To investigate this point in more detail, the *C*-*V* characteristics of the diode were measured.

Figure 8A shows the measured C^{-2}-*V* plot of P-ion-implanted n-$BaSi_2$/p-Si heterojunction solar cells annealed at 500°C for 120 s together with that simulated by AFORS-HET from the band alignment shown in Figure 1B. The intercept of the linear plot corresponding to the built-in voltage (V_{bi}) in the case of a one-sided abrupt junction was thus measured to be 0.52 V. This value was much smaller than the simulated value of 0.82 V. Therefore, the actual band alignment is

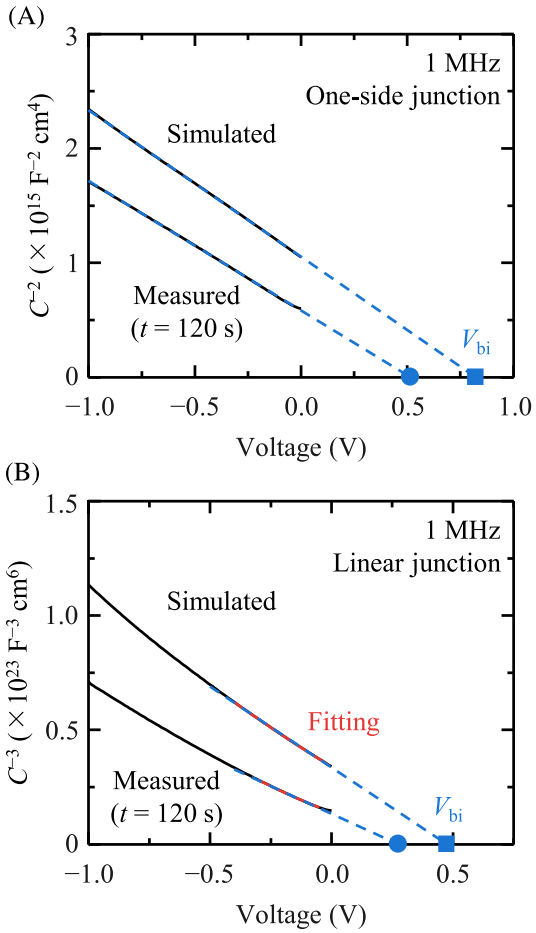

FIGURE 8 (A) C^{-2}-*V* and (B) C^{-3}-*V* plots of P-ion-implanted n-$BaSi_2$/p-Si heterojunction solar cells annealed at 500°C for 120 s. Simulation results by AFORS-HET are also shown. [Colour figure can be viewed at wileyonlinelibrary.com]

different from that in Figure 1B probably due to defects at the n-$BaSi_2$/p-Si heterointerface. As discussed later, since the P concentration was not uniform in the $BaSi_2$ film, the case of a linearly graded junction was also investigated. Figure 8B shows the measured and simulated C^{-3}-*V* plots. The measured V_{bi} of 0.28 V was also much smaller than that simulated (0.48 V). Hydrogen passivation may be one way to improve interface properties; however, we have no information to discuss further at present, and thus further studies are mandatory. We next discuss the values of R_S and R_{SH}. The R_S of the diode in this work is about one order of magnitude greater than that of n-

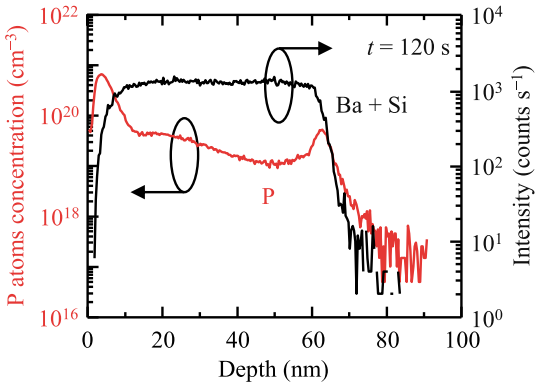

FIGURE 9 SIMS depth profiles of P atoms concentration and secondary ions (Ba + Si) in P-ion-implanted n-$BaSi_2$/p-Si heterojunction solar cells annealed at 500°C for 120 s [Colour figure can be viewed at wileyonlinelibrary.com]

$BaSi_2$/p-Si solar cells using MBE-grown Sb-doped n-$BaSi_2$ layers (~100 Ω).[22] The electron concentration of P-ion-implanted n-$BaSi_2$ films ($n = 1.5 \times 10^{18}$ cm^{-3}) is one order of magnitude smaller than that of the Sb-doped n-$BaSi_2$ ($n = 1.0 \times 10^{19}$ cm^{-3}),[22] leading to a large contact resistance. In addition, the R_{SH} is 20–30 times smaller than that of the MBE-grown n-$BaSi_2$/p-Si solar cells (~1 MΩ).[22] From the depth profiles of P atoms (Figure 9) in the n-$BaSi_2$/p-Si heterojunction solar cells annealed for 120 s, the averaged P atoms concentration at depths of 10–60 nm from the surface was ~10^{19} cm^{-3}. Therefore, the activation rate of P atoms was approximately 10%. From this activation rate of P atoms and the N_C of $BaSi_2$,[30] the donor level of P atoms is calculated to be positioned approximately 0.12 eV from the conduction band minimum. The segregation of P atoms occurred in the surface region and around the $BaSi_2$/Si hetero-interface. We presume that these segregated P atoms deteriorate both the series resistance and shunt resistance. Therefore, a uniform distribution of P atoms in $BaSi_2$ films appears mandatory if these parameters are to be improved.

4 | CONCLUSION

We fabricated P-ion-implanted n-$BaSi_2$ films for use as $BaSi_2$/Si heterojunctions in solar cells. First, we determined the diffusion coefficient of P atoms in the lattice and GB of $BaSi_2$ and subsequently the activation energies, which we found to be 1.1 ± 0.6 and 2.5 ± 0.6 eV, respectively. Raman and PL spectra revealed that postannealing improved the crystalline quality and the optical properties of P-ion-implanted $BaSi_2$ films. The *IQE* reached a maximum of 67% at a wavelength of approximately 900 nm, which is the highest value of n-$BaSi_2$/p-Si heterojunction solar cells. Rectification in the *J*–*V* characteristics was achieved by these P-ion-implanted n-$BaSi_2$/p-Si heterojunction solar cells. We demonstrated that ion implantation is possible in the fabrication of $BaSi_2$ solar cells.

ACKNOWLEDGEMENTS

This work was financially supported in part by JSPS KAKENHI (Grants 19KK0104 and JP21H04548). A. S. and Y. Y. are financially supported by Grant-in-Aids for JSPS Research Fellowships for Young Scientists (Grant 21J20404 and 19J21372). We are grateful to the Scientific Grant Agency of the Ministry of Education, Science, Research and Sport of the Slovak Republic for financial support of projects VEGA 1/0532/19 and VEGA 1/0529/20.

DATA AVAILABILITY STATEMENT

The data that support the findings of this study are available from the corresponding author upon reasonable request.

ORCID

Sho Aonuki https://orcid.org/0000-0002-9155-9170
Yudai Yamashita https://orcid.org/0000-0003-0477-425X
Gianluca Limodio https://orcid.org/0000-0001-9257-8034
Shunsuke Narita https://orcid.org/0000-0001-7498-5365
Miro Zeman https://orcid.org/0000-0002-1710-360X
Olindo Isabella https://orcid.org/0000-0001-7673-0163
Takashi Suemasu https://orcid.org/0000-0001-6012-4986

REFERENCES

1. ©Fraunhofer ISE: Photovoltaics Report, updated: 24 February 2022.
2. Yoshikawa K, Kawasaki H, Yoshida W, et al. Silicon heterojunction solar cell with interdigitated back contacts for a photoconversion efficiency over 26%. *Nat Energy*. 2017;2(5):17032. doi:10.1038/nenergy.2017.32
3. Richter A, Müller R, Benick J, et al. Design rules for high-efficiency both-sides-contacted silicon solar cells with balanced charge carrier transport and recombination losses. *Nat Energy*. 2021;6(4):429-438. doi:10.1038/s41560-021-00805-w
4. Haase F, Hollemann C, Schäfer S, et al. Laser contact openings for local poly-Si-metal contacts enabling 26.1%-efficient POLO-IBC solar cells. *Sol Energy Mater sol Cells*. 2018;186:184-193. doi:10.1016/j.solmat.2018.06.020
5. Press Release, LONGi Green Energy Technology Co., Ltd. 2021. Accessed at 23 June 2022. https://www.longi.com/en/news/7469/on
6. Britt J, Ferekides C. Thin-film CdS/CdTe solar cell with 15.8% efficiency. *Appl Phys Lett*. 1993;62(22):2851-2852. doi:10.1063/1.109629
7. Romeo A, Terheggen M, Abou-Ras D, et al. Development of thin-film Cu(In,Ga)Se_2 and CdTe solar cells. *Prog Photovoltaics Res Appl*. 2004;12:93-111. doi:10.1002/pip.527
8. Wu X. High-efficiency polycrystalline CdTe thin-film solar cells. *Sol Energy*. 2004;77(6):803-814. doi:10.1016/j.solener.2004.06.006
9. Repins I, Contreras MA, Egaas B, et al. 19·9%-efficient ZnO/-CdS/CuInGaSe_2 solar cell with 81·2% fill factor. *Prog Photovoltaics Res Appl*. 2008;16(3):235-239. doi:10.1002/pip.822
10. Katagiri H, Jimbo K, Maw WS, et al. Development of CZTS-based thin film solar cells. *Thin Solid Films*. 2009;517(7):2455-2460. doi:10.1016/j.tsf.2008.11.002
11. Jackson P, Würz R, Rau U, et al. High quality baseline for high efficiency, Cu(In_{1-x},Ga_x)Se_2 solar cells. *Prog Photovoltaics Res Appl*. 2007;15:507-519. doi:10.1002/pip.757
12. Jackson P, Wuerz R, Hariskos D, et al. Effects of heavy alkali elements in Cu(In,Ga)Se_2 solar cells with efficiencies up to 22.6%. *Phys Status Solidi Rapid Res Lett*. 2016;10:583-586. doi:10.1002/pssr.201600199

13. Suemasu T, Migas DB. Recent progress toward realization of high-efficiency $BaSi_2$ solar cells: thin-film deposition techniques and passivation of defects. *Phys Status Solidi a*. 2022;219(1):2100593. doi:10.1002/pssa.202100593
14. Suemasu T, Usami N. Exploring the potential of semiconducting $BaSi_2$ for thin-film solar cell applications. *J Phys D Appl Phys*. 2017;50(2):023001. doi:10.1088/1361-6463/50/2/023001
15. Kumar M, Umezawa N, Zhou W, Imai M. Barium disilicide as a promising thin-film photovoltaic absorber: structural, electronic, and defect properties. *J Mater Chem a*. 2017;5(48):25293-25302. doi:10.1039/c7ta08312b
16. Toh K, Saito T, Suemasu T. Optical absorption properties of $BaSi_2$ epitaxial films grown on a transparent silicon-on-insulator substrate using molecular beam epitaxy. *Jpn J Appl Phys*. 2011;50(6):068001. doi:10.1143/JJAP.50.068001
17. Baba M, Watanabe K, Hara KO, et al. Evaluation of minority carrier diffusion length of undoped n-$BaSi_2$ epitaxial thin films on Si(001) substrates by electron-beam-induced-current technique. *Jpn J Appl Phys*. 2014;53(7):078004. doi:10.7567/JJAP.53.078004
18. Baba M, Toh K, Toko K, et al. Investigation of grain boundaries in $BaSi_2$ epitaxial films on Si(111) substrates using transmission electron microscopy and electron-beam-induced current technique. *J Cryst Growth*. 2012;348(1):75-79. doi:10.1016/j.jcrysgro.2012.03.044
19. Yachi S, Takabe R, Takeuchi H, Toko K, Suemasu T. Effect of amorphous Si capping layer on the hole transport properties of $BaSi_2$ and improved conversion efficiency approaching 10% in p-$BaSi_2$/n-Si solar cells. *Appl Phys Lett*. 2016;109(7):072103. doi:10.1063/1.4961309
20. Yachi S, Takabe R, Toko K, Suemasu T. Effect of p-$BaSi_2$ layer thickness on the solar cell performance of p-$BaSi_2$/n-Si heterojunction solar cells. *Jpn J Appl Phys*. 2017;56(5S1):05DB03. doi:10.7567/JJAP.56.05DB03
21. Deng T, Sato T, Xu Z, et al. P-$BaSi_2$/n-Si heterojunction solar cells on Si(001) with conversion efficiency approaching 10%: comparison with Si(111). *Appl Phys Express*. 2018;11(6):062301. doi:10.7567/APEX.11.062301
22. Kodama K, Takabe R, Deng T, Toko K, Suemasu T. Spectroscopic evidence of photogenerated carrier separation by built-in electric field in Sb-doped n-$BaSi_2$/B-doped p-$BaSi_2$ homojunction diodes. *Jpn J Appl Phys*. 2018;57(5):050310. doi:10.7567/JJAP.57.050310
23. Yamashita Y, Ruiz Tobon CM, Santbergen R, Zeman M, Isabella O, Suemasu T. Solar cells based on n^+-AZO/p-$BaSi_2$ heterojunction: advanced opto-electrical modelling and experimental demonstration. *Sol Energy Mater sol Cells*. 2021;230:111181. doi:10.1016/j.solmat.2021.111181
24. Fujiwara M, Takahashi K, Nakagawa Y, et al. Improved conversion efficiency of p-type $BaSi_2$/n-type crystalline Si heterojunction solar cells by a low growth rate deposition of $BaSi_2$. *AIP Adv*. 2022;12(4):045115. doi:10.1063/5.0083812
25. Kodama K, Yamashita Y, Toko K, Suemasu T. Operation of $BaSi_2$ homojunction solar cells on p^+-Si(111) substrates and the effect of structure parameters on their performance. *Appl Phys Express*. 2019;12(4):041005. doi:10.7567/1882-0786/ab0c4f
26. Suemasu T. Exploring the possibility of semiconducting $BaSi_2$ for thin-film solar cell applications. *Jpn J Appl Phys*. 2015;54(7S2):07JA01. doi:10.7567/JJAP.54.07JA01
27. Koitabashi R, Nemoto T, Yamashita Y, Mesuda M, Toko K, Suemasu T. Formation of high-photoresponsivity $BaSi_2$ films on glass substrate by radio-frequency sputtering for solar cell applications. *J Phys D Appl Phys*. 2021;54(13):135106. doi:10.1088/1361-6463/abd434
28. Zhang N, Nakamura K, Baba M, Toko K, Suemasu T. Diffusion coefficients of impurity atoms in $BaSi_2$ epitaxial films grown by molecular beam epitaxy. *Jpn J Appl Phys*. 2014;53(4S):04ER02. doi:10.7567/JJAP.53.04ER02
29. Kobayashi M, Matsumoto Y, Ichikawa Y, Tsukada D, Suemasu T. Control of electron and hole concentrations in semiconducting silicide $BaSi_2$ with impurities grown by molecular beam epitaxy. *Appl Phys Express*. 2008;1:051403. doi:10.1143/APEX.1.051403
30. Migas DB, Shaposhnikov VL, Borisenko VE. Isostructural $BaSi_2$, $BaGe_2$ and $SrGe_2$: electronic and optical properties. *Phys Status Solidi B*. 2007;244(7):2611-2618. doi:10.1002/pssb.200642556
31. Kumar M, Umezawa N, Imai M. $BaSi_2$ as a promising low-cost, earth-abundant material with large optical activity for thin-film solar cells: a hybrid density functional study. *Appl Phys Express*. 2014;7(7):071203. doi:10.7567/APEX.7.071203
32. Imai Y, Watanabe A, Mukaida M. Electronic structures of semiconducting alkaline-earth metal silicides. *J Alloys Compd*. 2003;358(1-2):257-263. doi:10.1016/S0925-8388(03)00037-9
33. Kumar M, Umezawa N, Imai M. $(Sr,Ba)(Si,Ge)_2$ for thin-film solar-cell applications: first-principles study. *J Appl Phys*. 2014;115:203718. doi:10.1063/1.4880662
34. Aonuki S, Yamashita Y, Toko K, Suemasu T. Fabrication of As-doped n-type $BaSi_2$ epitaxial films grown by molecular beam epitaxy. *Jpn J Appl Phys*. 2020;59(SF):SFFA01. doi:10.7567/1347-4065/ab5b7a
35. Aonuki S, Yamashita Y, Toko K, Suemasu T. Effects of Ba-to-Si deposition rate ratios on the electrical and photoresponse properties of arsenic-doped n-type $BaSi_2$ films. *Thin Solid Films*. 2021;738:138969. doi:10.1016/j.tsf.2021.138969
36. Aonuki S, Yamashita Y, Sato T, et al. Significant enhancement of photoresponsivity in As-doped n-$BaSi_2$ epitaxial films by atomic hydrogen passivation. *Appl Phys Express*. 2020;13(5):051001. doi:10.35848/1882-0786/ab8725
37. Aonuki S, Xu Z, Yamashita Y, et al. Mechanisms of carrier lifetime enhancement and conductivity-type switching on hydrogen-incorporated arsenic-doped $BaSi_2$. *Thin Solid Films*. 2021;724:138629. doi:10.1016/j.tsf.2021.138629
38. Hara KO, Hoshi Y, Usami N, et al. N-type doping of $BaSi_2$ epitaxial films by phosphorus ion implantation and thermal annealing. *Thin Solid Films*. 2014;557:90-93. doi:10.1016/j.tsf.2013.08.038
39. Hara KO, Usami N, Baba M, Toko K, Suemasu T. N-type doping of $BaSi_2$ epitaxial films by arsenic ion implantation through a dose-dependent carrier generation mechanism. *Thin Solid Films*. 2014;567:105-108. doi:10.1016/j.tsf.2014.07.049
40. Takabe R, Baba M, Nakamura K, et al. Fabrication and characterizations of phosphorus-doped n-type $BaSi_2$ epitaxial films grown by molecular beam epitaxy. *Phys Status Solidi C*. 2013;10(12):1753-1755. doi:10.1002/pssc.201300326
41. Varache R, Leendertz C, Gueunier-Farret ME, Haschke J, Muñoz D, Korte L. Investigation of selective junctions using a newly developed tunnel current model for solar cell applications. *Sol Energy Mater sol Cells*. 2015;141:14-23. doi:10.1016/j.solmat.2015.05.014
42. Suemasu T, Morita K, Kobayashi M, Saida M, Sasaki M. Band diagrams of $BaSi_2$/Si structure by kelvin probe and current-voltage characteristics. *Jpn J Appl Phys*. 2006;45(20):L519-L521. doi:10.1143/JJAP.45.L519
43. Inomata Y, Nakamura T, Suemasu T, Hasegawa F. Epitaxial growth of semiconducting $BaSi_2$ thin films on Si(111) substrates by reactive deposition epitaxy. *Jpn J Appl Phys*. 2004;43(7A):4155-4156. doi:10.1143/JJAP.43.4155
44. Inomata Y, Nakamura T, Suemasu T, Hasegawa F. Epitaxial growth of semiconducting $BaSi_2$ films on Si(111) substrates by molecular beam epitaxy. *Jpn J Appl Phys*. 2004;43(4A):L478-L481. doi:10.1143/JJAP.43.L478
45. Suemasu T, Hara KO, Udono H, Imai M. Silicon meets group-II metals in energy and electronic applications—how to handle reactive sources for high-quality films and bulk crystals. *J Appl Phys*. 2022;131(19):191101. doi:10.1063/5.0092080

46. Takabe R, Takeuchi H, Du W, et al. Evaluation of band offset at amorphous-Si/$BaSi_2$ interfaces by hard X-ray photoelectron spectroscopy. *J Appl Phys*. 2016;119(16):165304. doi:10.1063/1.4947501
47. Suhara T, Murata K, Navabi A, et al. Postannealing effects on undoped $BaSi_2$ evaporated films grown on Si substrates. *Jpn J Appl Phys*. 2017;56(5S1):05DB05. doi:10.7567/JJAP.56.05DB05
48. Haku Y, Aonuki S, Yamashita Y, Toko K, Suemasu T. Effect of post-annealing on the significant photoresponsivity enhancement of $BaSi_2$ epitaxial films on Si(111). *Appl Phys Express*. 2021;14(2):021003. doi:10.35848/1882-0786/abdc9f
49. Narita S, Yamashita Y, Aonuki S, Saitoh N, Toko K, Suemasu T. High-temperature post-annealing effect on the surface morphology and photoresponse and electrical properties of B-doped $BaSi_2$ films grown by molecular beam epitaxy under various Ba-to-Si deposition rate ratios. *J Cryst Growth*. 2022;578:126429. doi:10.1016/j.jcrysgro.2021.126429
50. van der Pauw LJ. A method of measuring specific resistivity and Hall effect of discs of arbitrary shape. *Semicond Devices Pioneer Pap*. 1991;13:174-182. doi:10.1142/9789814503464_0017
51. Belova IV, Murch GE. Analysis of kinetics regimes in grain boundary self-diffusion. *Philos Mag*. 2009;89(7):665-675. doi:10.1080/14786430802555714
52. Whipple RTP. CXXXVIII. Concentration contours in grain boundary diffusion. *Lond Edinb Dublin Philos Mag J Sci*. 1954;45(371):1225-1236. doi:10.1080/14786441208561131
53. Belova IV, Fiedler T, Kulkarni N, Murch GE. The Harrison diffusion kinetics regimes in solute grain boundary diffusion. *Philos Mag*. 2012;92(14):1748-1763. doi:10.1080/14786435.2012.657710
54. Harrison LG. Influence of dislocations on diffusion kinetics in solids with particular reference to the alkali halides. *Trans Faraday Soc*. 1961;57:1191-1199. doi:10.1039/TF9615701191
55. Le Claire AD. The analysis of grain boundary diffusion measurements. *Br J Appl Phys*. 1963;14(6):351-356. doi:10.1088/0508-3443/14/6/317
56. Baba M, Nakamura K, Du W, et al. Molecular beam epitaxy of $BaSi_2$ films with grain size over 4μm on Si(111). *Jpn J Appl Phys*. 2012;51:098003. doi:10.1143/JJAP.51.098003
57. Nakamura K, Baba M, Ajmal Khan M, et al. Lattice and grain-boundary diffusions of boron atoms in $BaSi_2$ epitaxial films on Si(111). *J Appl Phys*. 2013;113(5):053511. doi:10.1063/1.4790597
58. Nakamura K, Toh K, Baba M, et al. Lattice and grain-boundary diffusions of impurity atoms in $BaSi_2$ epitaxial layers grown by molecular beam epitaxy. *J Cryst Growth*. 2013;378:189-192. doi:10.1016/j.jcrysgro.2012.12.051
59. Zhang N, Nakamura K, Baba M, Toko K, Suemasu T. Evaluation of diffusion coefficients of n-type impurities in MBE-grown $BaSi_2$ epitaxial layers. *Phys Status Solidi Curr Top Solid State Phys*. 2013;10(12):1762-1764. doi:10.1002/pssc.201300334
60. Bokstein BS, Fradkov VE, Beke DL. Grain boundary segregation and grain-boundary heterodiffusion. *Philos Mag a*. 1992;65(2):277-286. doi:10.1080/01418619208201523
61. Mishin Y, Herzig C, Bernardini J, Gust W. Grain boundary diffusion: fundamentals to recent developments. *Int Mater Rev*. 1997;42(4):155-178. doi:10.1179/imr.1997.42.4.155
62. Sze SM. *Physics of Semiconductor Devices*. 2nd ed. New York: Wiley; 1981.
63. Takabe R, Deng T, Kodama K, et al. Impact of Ba to Si deposition rate ratios during molecular beam epitaxy on carrier concentration and spectral response of $BaSi_2$ epitaxial films. *J Appl Phys*. 2018;123(4):045703. doi:10.1063/1.4994850
64. Sato T, Hoshida H, Takabe R, Toko K, Terai Y, Suemasu T. Detection of local vibrational modes induced by intrinsic defects in undoped $BaSi_2$ light absorber layers using Raman spectroscopy. *J Appl Phys*. 2018;124(2):025301. doi:10.1063/1.5029320
65. Xu Z, Sato T, Benincasa L, et al. Atomic hydrogen passivation for photoresponsivity enhancement of boron-doped p-$BaSi_2$ films and performance improvement of boron-doped p-$BaSi_2$/n-Si heterojunction solar cells. *J Appl Phys*. 2020;127(23):233104. doi:10.1063/5.0005763
66. Sato T, Yamashita Y, Xu Z, et al. Correlation of native defects between epitaxial films and polycrystalline $BaSi_2$ bulks based on photoluminescence spectra. *Appl Phys Express*. 2019;12(11):111001. doi:10.7567/1882-0786/ab476f
67. Nemoto T, Aonuki S, Koitabashi R, et al. Solar cell operation of sputter-deposited n-$BaSi_2$/p-Si heterojunction diodes and characterization of defects by deep-level transient spectroscopy. *Appl Phys Express*. 2021;14(5):051010. doi:10.35848/1882-0786/abfb87
68. Sites JR, Mauk PH. Diode quality factor determination for thin-film solar cells. *Sol Cells*. 1989;27(1-4):411-417. doi:10.1016/0379-6787(89)90050-1
69. Lu M, Das U, Bowden S, et al. Optimization of interdigitated back contact silicon heterojunction solar cells: tailoring hetero-interface band structures while maintaining surface passivation. *Prog Photovoltaics Res Appl*. 2011;19(3):326-338. doi:10.1002/pip.1032
70. Das U, Hegedus S, Zhang L, et al. Investigation of hetero-interface and junction properties in silicon heterojunction solar cells. In: *2010 35th IEEE Photovoltaic Specialists Conference*. IEEE; 2010:1358-1362. doi:10.1109/PVSC.2010.5614372
71. Ecker B, Egelhaaf H-J, Steim R, et al. Understanding S-shaped current–voltage characteristics in organic solar cells containing a TiO_x interlayer with impedance spectroscopy and equivalent circuit analysis. *J Phys Chem C*. 2012;116:16333-16337. doi:10.1021/jp305206d

How to cite this article: Aonuki S, Yamashita Y, Limodio G, et al. Device operation of P-ion-implanted n-$BaSi_2$/p-Si heterojunction solar cells. *Prog Photovolt Res Appl*. 2022;1-9. doi:10.1002/pip.3658